

TUNeS: A Temporal U-Net with Self-Attention for Video-based Surgical Phase Recognition

Isabel Funke, Dominik Rivoir, Stefanie Krell, and Stefanie Speidel, *Member, IEEE*

arXiv:2307.09997v1 [cs.CV] 19 Jul 2023

Abstract— To enable context-aware computer assistance in the operating room of the future, cognitive systems need to understand automatically which surgical phase is being performed by the medical team. The primary source of information for surgical phase recognition is typically video, which presents two challenges: extracting meaningful features from the video stream and effectively modeling temporal information in the sequence of visual features. For temporal modeling, attention mechanisms have gained popularity due to their ability to capture long-range dependencies. In this paper, we explore design choices for attention in existing temporal models for surgical phase recognition and propose a novel approach that does not resort to local attention or regularization of attention weights: TUNeS is an efficient and simple temporal model that incorporates self-attention at the coarsest stage of a U-Net-like structure. In addition, we propose to train the feature extractor, a standard CNN, together with an LSTM on preferably long video segments, i.e., with long temporal context. In our experiments, all temporal models performed better on top of feature extractors that were trained with longer temporal context. On top of these contextualized features, TUNeS achieves state-of-the-art results on Cholec80.

Index Terms— action segmentation, attention, Cholec80, sequence modeling, surgical phase, surgical workflow

I. INTRODUCTION

Video-based surgical phase recognition refers to automatically analyzing the video stream that is recorded in the operating room to recognize which surgical phase [1] is being performed. Robust and accurate methods for surgical phase

This work has been submitted to the IEEE for possible publication. Copyright may be transferred without notice, after which this version may no longer be accessible.

Partially funded by the German Research Foundation (DFG, Deutsche Forschungsgemeinschaft) as part of Germany's Excellence Strategy – EXC 2050/1 – Project ID 390696704 – Cluster of Excellence "Centre for Tactile Internet with Human-in-the-Loop" (CeTI) of Technische Universität Dresden. The authors acknowledge the financial support by the Federal Ministry of Education and Research of Germany in the programme of "Souverän. Digital. Vernetzt.". Joint project 6G-life, project identification number: 16KISK001K. (*Corresponding author: Isabel Funke.*)

I. Funke, D. Rivoir, S. Krell, and S. Speidel are with the Department of Translational Surgical Oncology, National Center for Tumor Diseases (NCT/UCC), Dresden, Germany; German Cancer Research Center (DKFZ), Heidelberg, Germany; Carl Gustav Carus Faculty of Medicine and University Hospital, TUD Dresden University of Technology, Dresden, Germany; Helmholtz-Zentrum Dresden-Rossendorf (HZDR), Dresden, Germany.

I. Funke, D. Rivoir, and S. Speidel are with the Centre for Tactile Internet with Human-in-the-Loop (CeTI), TUD Dresden University of Technology, Dresden, Germany.

recognition are a prerequisite for computer-assisted surgery, where context-aware assistance functions are to be provided automatically [2]. Such intra-operative assistance functions could comprise, e.g., providing crucial patient-related information at the right time or monitoring the operation to issue early warnings in case of hazardous events. In addition, the video could be analyzed in full after the surgery, for example to automatically create a surgical report or to estimate the risk of post-operative complications. Such post-operative analyses rely on methods for surgical phase recognition as well.

Current approaches to the task of surgical phase recognition follow a data-driven approach, meaning that they learn from annotated example videos how to perform the task. Typically, two types of deep-learning models are employed: (1) a visual feature extractor, such as a *Convolutional Neural Network (CNN)* or a *Vision Transformer* [3], and (2) a temporal model, such as a *Temporal Convolutional Network (TCN)* [4], [5] or a *Recurrent Neural Network (RNN)*, where the latter typically consists of *Long Short-Term Memory (LSTM)* cells [6] or *Gated Recurrent Units (GRUs)* [7]. Here, the visual feature extractor learns to extract descriptive features from individual video frames. Given the sequence of extracted visual features, the temporal model learns to identify meaningful temporal patterns, dependencies, and relations in the sequence to infer the surgical phase at any time.

To build a model that can accurately identify phases in long surgical videos, two aspects are crucial: obtaining meaningful visual features that can be easily analyzed and designing the temporal model to capture long-range temporal relationships. Both of these aspects still pose considerable challenges.

1) *Visual feature extraction*: The question of how to obtain suitable visual features for phase recognition has not been studied extensively so far. Most methods simply finetune a CNN, typically a *ResNet* [8], on the task of phase recognition after pre-training on a large-scale dataset like *ImageNet* [9]. Few studies [10], [11] investigated other architectures for feature extraction, such as a *Swin Vision Transformer* [12] or spatio-temporal video models like *X3D* [13] and *Video Swin Transformer* [14]. Others explored training a standard CNN either on additional tasks, e.g., tool recognition [15], [16], surgical step recognition [17], or surgical scene segmentation [18], or on self-supervised objectives [19]–[21].

Inspired by the performance of simple end-to-end CNN-LSTM models on the phase recognition task [22], [23], we propose to train the feature extractor, a standard CNN, in context by combining it with an LSTM network and training

both components jointly on short video sequences (up to 64 frames) (see section III-A, Fig. 4). Training with temporal context rewards the CNN to extract features that could prove useful in hindsight and enables the CNN to tolerate ambiguous frames, relying on the LSTM to resolve these. After training, features are extracted using the CNN only.

2) *Modeling long-range relationships: Attention mechanisms* [24] were designed to model global relations in sequences. Here, the output at time t is a function of all feature vectors in the sequence, regardless of their temporal distance to t , but weighted according to their relevance. By stacking attention mechanisms and feedforward neural networks, the *Transformer* architecture [25] achieved break-through results on sequence modeling tasks. Inspired by this success, researchers incorporated attention in temporal models for phase recognition [26]–[29] (see section II-D, Fig. 3). Yet, applying attention mechanisms to long, noisy sequences of visual features is not necessarily effective. Consequently, some methods had to revert to *local* attention, which is computed within limited time windows only – thus counteracting the idea of modeling global dependencies. In addition, the naive application of attention can induce high computational cost in terms of allocated GPU memory and computation time.

To overcome these limitations, we propose a novel, conceptually simple, computationally light-weight temporal model, where global attention is computed at the bottleneck of a *U-Net*-like [30], [31] encoder-decoder architecture (see section III-B, Fig. 5). The proposed model, named *TUNeS* (*Temporal U-Net with Self-Attention*), analyzes the feature sequence at several temporal scales and computes attention only at the coarsest scale, where high-level, semantically rich features are available. *TUNeS* is suited for both online and offline phase recognition.

3) *Evaluation*: We conducted a large number of experiments to demonstrate the positive effects of training the feature extractor with long temporal context (see section IV, Fig. 1). Our experiments also show that the proposed *TUNeS* model compares favorably to many baseline methods, both in terms of recognition accuracy and computational efficiency (Fig. 1 and Fig. 9). *TUNeS*, combined with a feature extractor that is trained with long temporal context, achieves state-of-the-art results on Cholec80. Source code will be made available.

II. BACKGROUND

A. Surgical phase recognition

Given a video v of length T , phase recognition is the task to estimate which phase p is being executed at any time t , where $1 \leq t \leq T$. Here, p is one of C predefined surgical phases. We denote the true phase that is happening at time t as y_t , $1 \leq y_t \leq C$, and the sequence of all ground truth phase labels as $(y_t)_{1 \leq t \leq T}$ or simply $y_{1:T}$. The estimate of the phase at time t , computed by a phase recognition algorithm, is $\hat{y}_t \in \mathbb{R}^C$, where $\hat{y}_{t,p}$ is the computed score (i.e., the logarithm of the unnormalized probability) for the event that y_t equals p , $1 \leq p \leq C$. The video itself is a sequence of video frames v_t .

For intra-operative applications, *online* phase recognition needs to be performed. In this case, only video frames $v_{t'}$ up

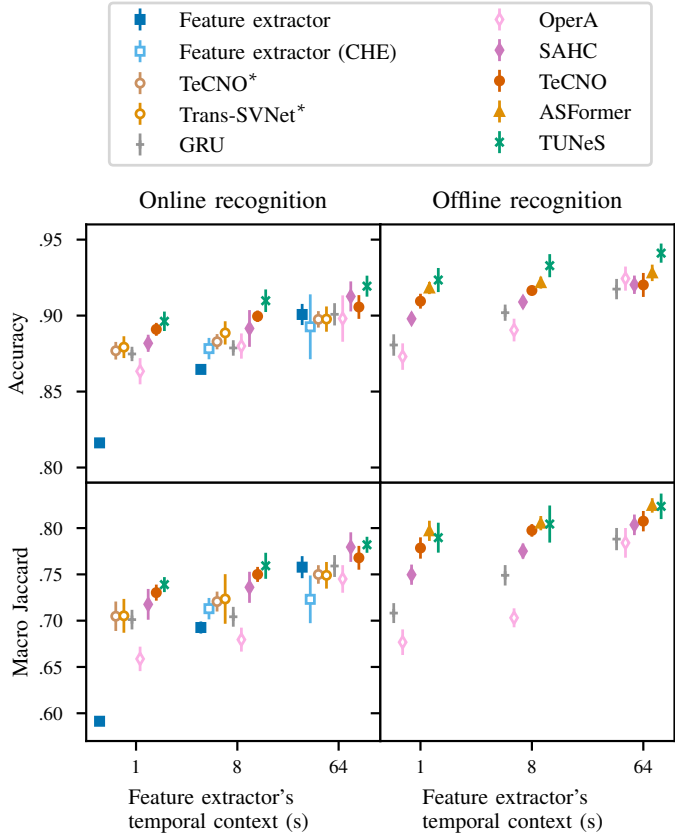


Fig. 1. Surgical phase recognition results on the Cholec80 dataset (32:8:40 split). Error bars indicate the standard deviation over repeated experimental runs. All temporal models perform better on top of feature extractors that were trained with longer temporal context L . * indicates that the temporal model was trained without feature sequence augmentation and smoothing loss. *TUNeS*, a temporal *U-Net* with self-attention, is introduced in this paper. As feature extractor, we employ a CNN, which is trained either on individual video frames ($L = 1$) or together with an LSTM network on sequences of L consecutive video frames.

until the current time, i.e., $t' \leq t$, can be analyzed to estimate the current phase. For post-operative applications, however, *offline* recognition is sufficient. In this case, information from all frames in the video can be processed to estimate the phase at any time in the video.

B. Attention mechanism

Let $Q = q_{1:S}$ be a sequence of *queries* and $U = u_{1:T}$ be a sequence of *values*, which is associated with a sequence $K = k_{1:T}$ of *keys*, i.e., k_t is the key of u_t for $1 \leq t \leq T$. In an attention mechanism [24], each element $q_s \in Q$ collects information from any element $u_t \in U$ by computing an attention-weighted sum over the complete sequence U :

$$\text{Attention}(Q, K, U) = (x_s)_{1 \leq s \leq S}, \text{ where} \\ x_s = \sum_t \frac{\exp \alpha(q_s, k_t)}{\sum_{t'} \exp \alpha(q_s, k_{t'})} \cdot u_t \quad (1)$$

The weights in this sum are the attention weights $\alpha(q_s, k_t)$ after Softmax normalization. These attention weights determine how relevant the element u_t is given query q_s . Based on [25], attention weights are computed as

$$\alpha(q_s, k_t) = (q_s^T k_t) / \sqrt{\dim}, \quad (2)$$

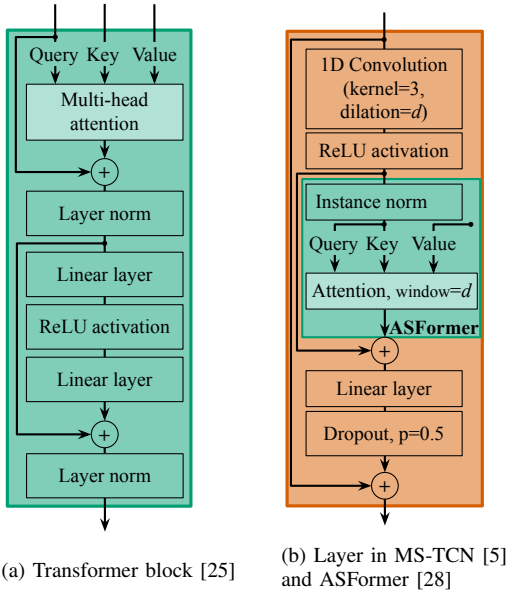


Fig. 2. Building blocks of related architectures. *ASFormer* adds an attention mechanism between the convolution and the fully connected layer of the *MS-TCN* layer.

where dim refers to the dimension of the vectors q_s and k_t .

In practice, Q , K , and U are each passed through a linear layer before computing attention. The parameters of these layers are learned so that the sequences are mapped to meaningful representations, where attention can be computed effectively. In *multi-head* attention [25], multiple linear layers are used, so attention will be computed on multiple representation subspaces in parallel. In the case of *self-attention*, Q , K , and U all refer to the same sequence.

Attention weights may be *masked*, i.e., set to $-\infty$, according to specific rules: *Local* attention is only computed within local time windows of size $1+2\omega$, i.e., $\alpha(q_s, k_t) = -\infty$ for all t with $|t-s| > \omega$. *Causal* attention does not allow attending to future sequence elements, thus $\alpha(q_s, k_t) = -\infty$ for all t with $t > s$.

In the Transformer architecture [25], attention is embedded in *Transformer blocks* with residual connections and normalization layers (Fig. 2a). The attention mechanism is followed by a feedforward network, which consists of two linear layers with a nonlinearity, e.g., ReLU or GELU [32], in between.

C. Models for surgical phase recognition

Early deep-learning models for video-based phase recognition consisted of a CNN for feature extraction and an LSTM network for temporal modeling [33, chapter 6.4]. Later, Czempiel *et al.* [16] proposed to use *TeCNO*, a *multi-stage TCN (MS-TCN)* [5], as temporal model. The model consists of multiple stages, where each stage consists of several layers with *dilated* [34] temporal convolutions (i.e., 1D convolutions along the temporal dimension), see Fig. 2b. To increase the receptive field, the dilation factor doubles at each layer. Subsequent stages are meant to refine the predictions of the previous stages. For online recognition, *causal* dilated convolutions [35] are used, meaning that convolutions are computed over the current and preceding time steps only. Yi *et al.* [36]

suggested to train such multi-stage models *not end-to-end*, but to apply disturbances to the intermediate feature sequences during training. Recently, Kadkhodamohammadi *et al.* [37] introduced *PATG*, which uses a *SE-ResNet* [38] as feature extractor and a graph neural network as temporal model. Zhang *et al.* [39] proposed a reinforcement learning approach to retrieve phase transitions for offline recognition.

Whereas feature extractor and temporal model were trained separately in these studies, others proposed to train both models jointly on truncated video sequences. In their pioneering work, Jin *et al.* [22] trained *SV-RCNet*, a ResNet-LSTM, end-to-end on video sequences with a duration of 2 s. Later, they proposed *TMRNet* [40], which augments a *ResNeSt-LSTM* [41] with a long-range memory bank [42] so that feature vectors from the previous 30 s can be queried to infer the current phase. Recently, Rivoir *et al.* [23] showed that CNN-LSTMs should be trained on even longer video sequences, while explicitly taking effects caused by *Batch Normalization (BN)* [43] into account. Their best model, a *ConvNeXt-LSTM* [44], is trained on sequences of 256 s.

In this paper, we also use an end-to-end CNN-LSTM to train the CNN, i.e., the visual feature extractor, with temporal context. To model global dependencies and for offline recognition, however, we propose to train a temporal model on the extracted feature sequences in a second step.

D. Temporal models with attention

Recent studies proposed to integrate attention mechanisms into temporal models for phase recognition (see Fig. 3). With attention, an element q_s in the *query* sequence can be related to any element u_t in the *value* sequence, regardless of their temporal distance $|t-s|$. In contrast, RNNs process a sequence sequentially, relying on their fixed-sized hidden state to retain the relevant information of previous sequence elements. Temporal convolutions, on the other hand, process information in a local neighborhood only. Thus, information needs to travel through several layers of convolutions to become available at temporally distant locations.

Czempiel *et al.* [26] presented *OperA*, a stack of Transformer blocks, for online recognition (Fig. 3b). This approach fully relies on self-attention to model temporal dependencies and thus may be lacking a notion of locality and temporal order. The model supposedly struggled to filter relevant information from the feature sequences, which can be noisy. Therefore, the authors proposed to train with a special attention regularization loss to make the model focus on relevant feature vectors.

Gao *et al.* [27] introduced *Trans-SVNet* for online recognition (Fig. 3c), which adds two Transformer blocks on top of a frozen *TeCNO* model. The first block computes self-attention on the *TeCNO* predictions. In the second block, the initial predictions of the feature extractor attend over the output of the first Transformer block. All attention operations are computed locally, using the feature vectors of the previous 30 s.

Yi *et al.* [28] proposed *ASFormer*, an offline model for temporal action segmentation (Fig. 3d). This model integrates attention into *MS-TCN* layers (Fig. 2b), thus interleaving convolutions, attention, and linear layers. Here, the convolutions

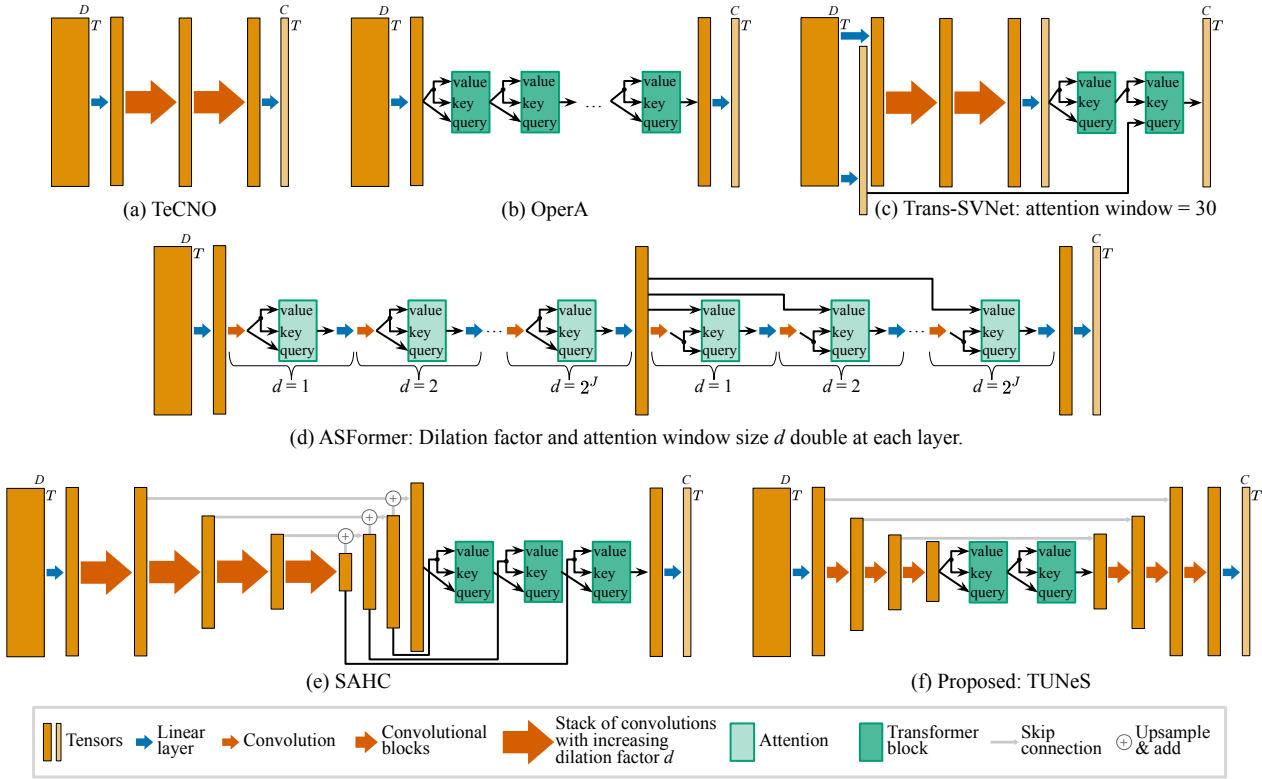


Fig. 3. Temporal models that process sequences of extracted visual features to obtain phase predictions $\hat{y}_{1:T}$. The dimension of extracted feature vectors is D . Different temporal models combine convolutions and attention in different ways.

help to encode a local inductive bias. Further, attention is computed within local windows, where the window size at each layer equals the dilation factor d of the convolution. Thus, within one stage, the attention window size doubles at each layer. Later, Zhang *et al.* [45] suggested to add a MS-TCN stage in parallel to the first ASFormer stage, and to fuse the outputs of both stages by concatenation. Chen *et al.* [46] presented an online two-stage version of ASFormer, where the dilation factors in the second stage are halved (instead of doubled) at each layer. As feature extractor, they used a Vision Transformer, *Twins-PCPVT* [47]. Restricting the attention to local neighborhoods of a predefined size seems to help with handling the complexity of long, noisy feature sequences but hinders the modeling of global dependencies.

In contrast to *implicitly* encoding hierarchical patterns into temporal models by using doubling dilation factors and attention windows, Ding and Li [29] proposed to explicitly use a hierarchical, multi-scale temporal model (Fig. 3e). SAHC uses MS-TCN-like stages to process feature sequences that are downsampled progressively. The computed multi-scale sequences are fused from coarse to fine (top-down), like in a *Feature Pyramid Network* [48]. Transformer blocks with global attention are integrated at the end of the model, where the final high-resolution sequence queries further information from the fused lower-resolution sequences, now proceeding from fine to coarse (bottom-up).

In this paper, we also propose a hierarchical temporal model, TUNeS (Fig. 3f). In contrast to SAHC, TUNeS follows a U-Net-like structure. We incorporate Transformer blocks at

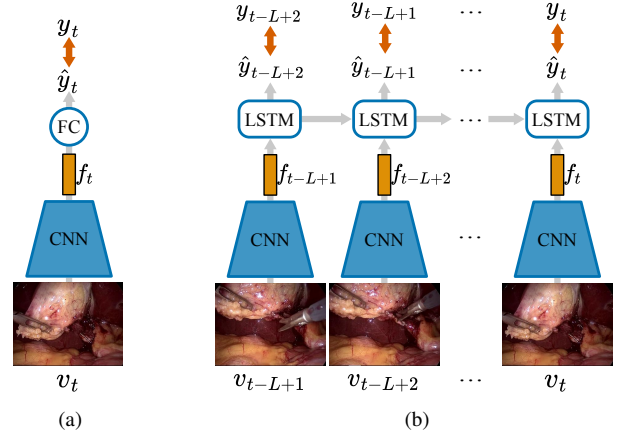


Fig. 4. Feature extractor training: (a) Training the CNN on individual video frames. The fully connected (FC) layer acts as linear classifier on top of the extracted feature vector f_t . (b) Training the CNN with *temporal context*, using an LSTM cell to model temporal relationships.

the core of our model, U-Net’s bottleneck, to model local and global temporal dependencies at the highest level of abstraction, using self-attention. In the decoder, the computed high-level semantic information is processed further and fused with the higher-resolution feature sequences from the encoder.

Previously, U-Nets with self-attention at the bottleneck were also used successfully for image generation with autoregressive models [49] or diffusion models [50], image segmentation [51], [52], and speech denoising [53].

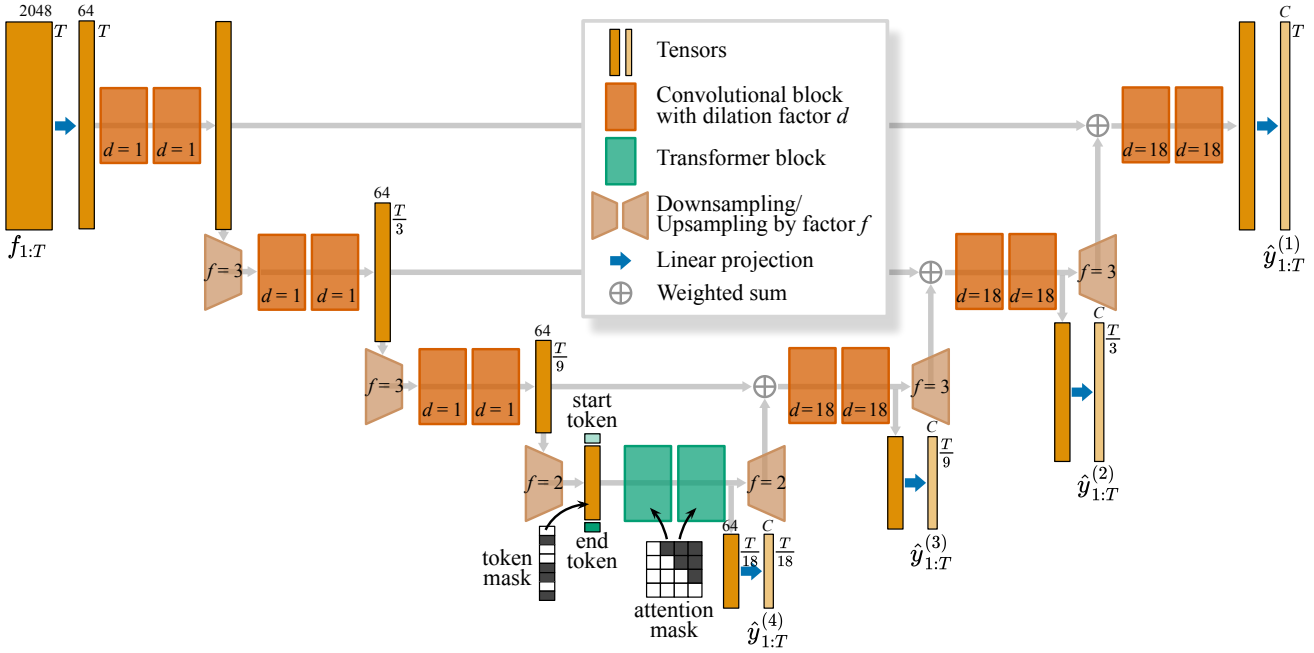


Fig. 5. Overview of the TUNeS architecture for online recognition. The sequence of feature vectors $f_{1:T}$ is analyzed at multiple temporal scales to obtain multi-scale phase predictions $\hat{y}_{1:T}^{(i)}$. Transformer blocks are integrated at the core of the architecture, computing self-attention.

III. METHODS

A. Feature extractor with temporal context

We use a standard CNN as feature extractor: ResNet-50, pre-trained on ImageNet. However, we train the CNN not on individual video frames (Fig. 4a) but with *temporal context*. For this purpose, we add an LSTM cell with 512 hidden units, which processes the sequence of computed CNN features. The CNN-LSTM is trained end-to-end on sequences of L consecutive frames (Fig. 4b). Here, we minimize the cross-entropy loss, computed on all L frames in the sequence.

To train on a class-balanced set of video sequences, we sample five sequences from each phase and one sequence around each phase transition from each video during one training epoch. After training, only the CNN is used to extract features: For each frame v_t , we obtain the feature vector $f_t \in \mathbb{R}^{2048}$ after the ResNet’s global average pooling layer.

To test the feature extractor’s recognition capabilities, we obtain the phase predictions of the jointly trained LSTM. In particular, to obtain the estimated phase at time t , we apply the CNN-LSTM to the sequence $(v_{t-L+i})_{1 \leq i \leq L}$ and take the final prediction \hat{y}_t . Thus, the LSTM is applied to L -frame sequences in a sliding window approach. In addition, we perform *carry-hidden evaluation (CHE)* [23], where the LSTM’s hidden state is carried through the video. Here, the LSTM is applied sequentially to the complete feature sequence.

B. Temporal U-Net with self-attention

TUNeS follows a U-Net-like encoder-decoder structure [30], [31] (Fig. 5). In the encoder, the feature sequence $f_{1:T}$ is repeatedly passed through temporal convolutions and downsampled. In the decoder, the sequence is repeatedly upsampled and passed through further convolutions. Down- and upsample

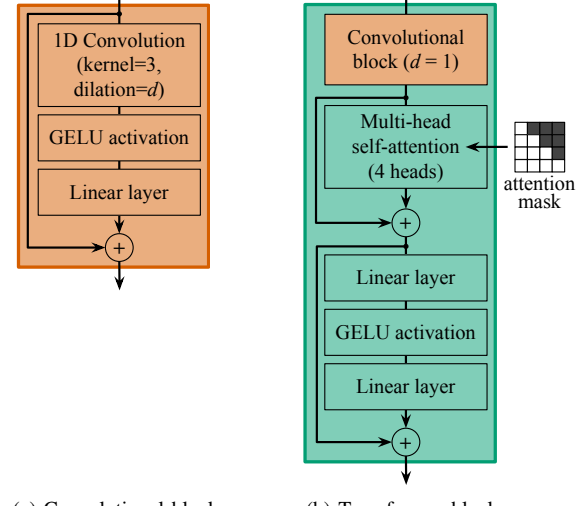


Fig. 6. TUNeS building blocks. All operations process and output sequences with $\text{dim} = 64$ channels or features. This also holds for each attention head in the Transformer block.

pling by factor f are implemented by 1D convolutions with kernel f and stride f , where the convolution is *transposed* [54] for upsampling. At the coarsest stage of the U-Net, Transformer blocks are used to model short-term and long-term temporal dependencies by computing global self-attention. Here, the downsampled feature sequence is interpreted as a sequence of *tokens*, to which additional start and end tokens are added.

By integrating Transformer blocks at the highest level of abstraction, TUNeS applies self-attention only to pre-filtered, semantically rich feature sequences of manageable length. In the decoder, the transformed high-level feature sequence is

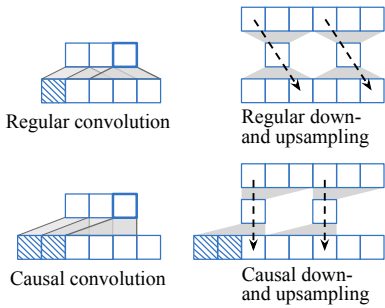


Fig. 7. Illustration of regular and causal convolutions (left) and down-sampling operations (right). Padded elements are depicted as cross-hatched squares. They are added at the beginning of a sequence to implement a shift to the right. Grey trapezoids relate inputs to outputs and thus indicate dependencies (\rightarrow) between sequence elements. In each subfigure, time proceeds from left to right and sequences are processed from bottom to top.

enriched with information of higher-resolution sequences by means of *skip connections* to the encoder. Here, the sum in each skip connection is weighted with a learnable scalar. Further, linear classifier heads at the end of each decoder stage compute phase predictions $\hat{y}^{(i)}$ at each temporal scale.

TUNeS consists mainly of convolutional blocks and Transformer blocks (Fig. 6). The convolutional block is similar to the MS-TCN layer. TUNeS uses regular convolutions without dilation ($d = 1$) in the encoder. In the decoder, dilated convolutions ($d = 18$) are used to retain a large receptive field when progressing to higher-resolution sequences. The Transformer block starts with a convolutional block to add local inductive bias [28]. This convolutional block could also be seen as ‘‘position encoding generator’’, which adds *conditional positional encodings* [55] to the input.

TUNeS uses the GELU activation function throughout the network and omits dropout regularization, which did not seem effective. Like MS-TCN, TUNeS does not include any normalization layers.

1) Causal operations for online recognition: To be applicable to online recognition, it is required that the temporal model does not access future information at any time. Therefore, TUNeS uses causal convolutions for online recognition, as previously proposed for TeCNO [16]. In addition, causal self-attention is computed in the Transformer blocks by applying a causal mask to the attention weights.

It is important to perform the downsampling operations in a causal way as well. Like for convolutions, this can be implemented by shifting input sequences by $k - 1$ elements to the right, where k is the size of the kernel (Fig. 7). In contrast, regular downsampling would leak future information. In that case, an element in the output sequence could depend on up to $k - 1$ future elements in the input sequence.

2) Separate future and past for offline recognition: When computing global self-attention in offline mode, it may be difficult to correctly separate past from future information. To help with this, we alternately prevent access to future and to past elements in the TUNeS Transformer blocks (Fig. 8). Further, we found it beneficial to increase the number of Transformer blocks for offline recognition from two to eight.

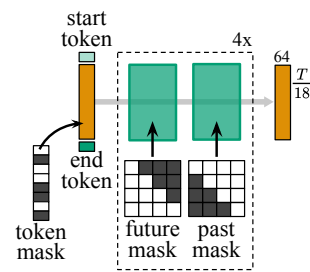


Fig. 8. For offline recognition, the Transformer blocks in TUNeS alternately process either information from the past or from the future.

3) Training objective: Let $\{\hat{y}^{(i)} : 1 \leq i \leq 4\}$ be the multi-scale phase predictions, where the length of each prediction $\hat{y}^{(i)}$ is reduced by factor χ_i and $\chi = (1, 3, 9, 18)$. For $2 \leq i \leq 4$, we compute downsampled ground truth annotations $y^{(i)}$ by applying one-hot encoding to y , followed by max pooling with kernel χ_i and stride χ_i . Thus, downsampled sequences will be annotated with multiple phases at times where a phase transition occurs.

We compute losses at all scales, using cross-entropy (CE) loss for the full-resolution prediction $\hat{y}^{(1)}$ and – due to the multi-label characteristics – binary cross-entropy (BCE) loss for the lower-resolution predictions, see (3).

$$\mathcal{L}_{\text{total}} = \mathcal{L}_{\text{phase}}(\hat{y}^{(1)}, y) + \sum_{k=2}^4 \mathcal{L}_{\text{BCE}}(\hat{y}^{(k)}, y^{(k)}) \quad (3)$$

$$\mathcal{L}_{\text{phase}}(\hat{y}, y) = \mathcal{L}_{\text{CE}}(\hat{y}, y) + \lambda_{\text{smooth}} \cdot \mathcal{L}_{\text{smooth}}(\hat{y})$$

To counter class imbalance, we use class weights γ in these losses, which are computed on the training data following the *median frequency balancing* [56] approach. In addition, we compute a *smoothing loss* [5] on the full-resolution prediction, which is weighted by factor $\lambda_{\text{smooth}} = 0.15$.

4) Regularization: For data augmentation, we augment feature sequences by (1) shifting the complete sequence to the right by a small random number of time steps and by (2) increasing and decreasing the video speed by randomly dropping and duplicating elements of the feature sequence.

In addition, we mask spans in the token sequences that are input to the Transformer blocks, inspired by the pre-training procedures for masked language models [57], [58]. Here, we randomly sample masks to cover spans that correspond to 18–300 s in the full-resolution video. However, we make sure that phase transitions are not masked because it would be impossible to reconstruct their exact timing. In total, around 35% of all tokens are masked per sequence.

IV. EXPERIMENTS

A. Dataset and evaluation metrics

All experiments were conducted on the *Cholec80* dataset [15]. Cholec80 consists of 80 video recordings of laparoscopic gallbladder removals, which are annotated with phase and tool information. We used only the phase annotations to train feature extractors and temporal models. The following $C = 7$ surgical phases are defined for Cholec80: (1) Preparation, (2) Calot triangle dissection, (3) Clipping and cutting, (4) Gallbladder dissection, (5) Gallbladder packaging, (6) Cleaning

and coagulation, and (7) Gallbladder retraction. Videos were processed at a temporal resolution of 1 fps in all experiments.

Unless stated otherwise, experiments were performed on the 32:8:40 data split, meaning that the first 32 videos in Cholec80 were used for training, the following eight videos for validation, and the last 40 videos for testing. In particular, hyperparameters were tuned on the validation subset.

We use the following evaluation metrics: Video-wise accuracy, video-wise Macro Jaccard (or Intersection over Union), and $F1$ score, which is computed as the harmonic mean of the mean video-wise Precision and the mean video-wise Recall. The Macro Jaccard for one test video is the average of the phase-wise Jaccard scores computed on this video. To avoid problems with undefined values, we omit the phase-wise scores for phase p and video v if p is not annotated in v .

For comparison with prior art, we also report the relaxed evaluation metrics \mathcal{R} -Jaccard (or \mathcal{R} -Precision and \mathcal{R} -Recall) and \mathcal{R} -Accuracy, which were proposed to tolerate certain errors within 10 s before or after an annotated phase transition. For all metrics, we used the implementations provided by [59].

B. Feature extractors

We trained feature extractors with context lengths L of one, eight, or 64 frames. Here, the feature extractor with $L = 1$ is simply a ResNet-50, without the LSTM on top (see Fig. 4a). Following the custom sampling strategy (section III-A), 1264 video sequences were processed in each epoch, for any size of L . With $L = 64$, we trained the feature extractor for 200 epochs. For comparability, we trained the feature extractor with $L = 8$ for 1600 epochs and with $L = 1$ for 12800 epochs. Thus, all feature extractors see the same amount of video frames during training, but in different contexts and in different order. The batch size was 10 video sequences with $L = 64$, 80 with $L = 8$, and 128 video frames with $L = 1$.

To account for the randomness in training deep-learning models, experiments were repeated five times using different random seeds.

C. Temporal models

For each context length $L \in \{1, 8, 64\}$, we trained TUNeS and a variety of other temporal models on the extracted feature sequences (see Fig. 1). The baseline temporal models included an RNN (2-layer GRU), a temporal convolutional network (TeCNO), and models that integrate attention in different ways (OperA, SAHC, ASFormer). Like for TUNeS, we set the hidden dimension of each baseline model to $\text{dim} = 64$. To account for random effects, we repeated each experiment five times on each of the five feature extractor instances, yielding 25 experimental runs in total.

All temporal models were trained for 75 epochs using the *Adam* [60] optimizer and a batch size of one feature sequence. Baseline models were trained on the combined loss $\mathcal{L}_{\text{phase}}$ (3) with $\lambda_{\text{smooth}} = 0.15$. For models with multiple stages (TeCNO, SAHC, ASFormer), we computed the loss on the output of all stages. Feature sequence augmentation was applied as described in section III-B.4. Gradients were clipped to have

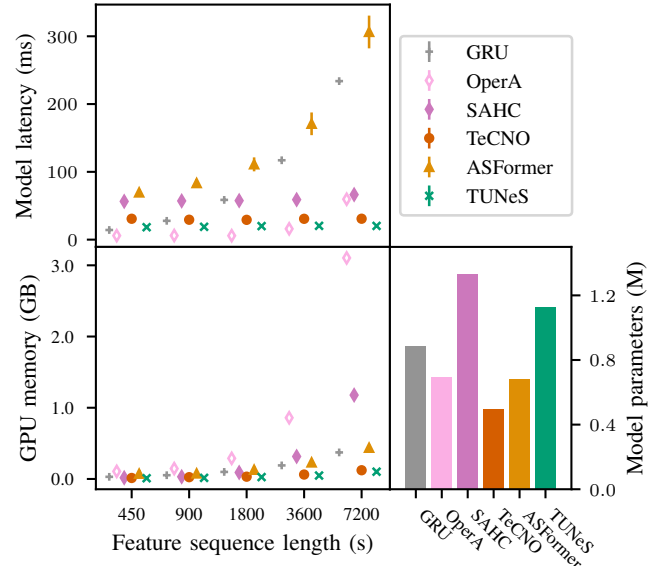


Fig. 9. Performance measurements for processing feature sequences of increasing duration with different temporal models in offline mode. Error bars indicate the standard deviation over measurements. Additionally, we present the number of parameters for each temporal model.

a maximum norm of 1. Finally, we selected the model that achieved the highest Macro Jaccard on the validation set.

In some cases, we also deviated from this training routine to accommodate the custom training strategy that was implemented in the original code base. To select an appropriate learning rate η for each baseline, we ran a quick sweep over $\eta \in \{1 \cdot 10^{-4}, 3 \cdot 10^{-4}, 5 \cdot 10^{-4}, 1 \cdot 10^{-3}\}$. In most cases, also for TUNeS, $\eta = 5 \cdot 10^{-4}$ worked well.

For TUNeS as well as for the baselines, we measured model latency and peak GPU memory allocation in offline mode on synthetic feature sequences with a length of 450, 900, 1800, 3600, and 7200 frames. Fig. 9 presents the mean of 1000 measurements, after taking 100 measurements for warm-up.

D. Comparison to the state of the art

We compare the results of TUNeS, trained on features with maximum context $L = 64$, with previously reported results on the 40:40 split (Tables I and II). Here, the feature extractor with $L = 64$ and TUNeS were re-trained on all of the first 40 videos in Cholec80. Due to the lack of a validation set, we selected the model after the last epoch for testing. To improve convergence, we continuously reduced the learning rate during training, following a cosine annealing schedule [61].

For comparisons on the 40:20:20 split, we did not perform additional training and tuning on the validation set. Instead, we simply evaluated the models trained for the 40:40 split on the last 20 videos in Cholec80.

E. Ablation studies

To further investigate properties of TUNeS, we repeated the experiments for $L = 64$ with the following modifications (see Fig. 10 and Fig. 11):

- Omit the convolutional block in the Transformer blocks

TABLE I

ONLINE RECOGNITION ON CHOLEC80 (40:40 SPLIT). COMPARISON TO RESULTS FROM THE LITERATURE.

Model	R-Accuracy		R-Jaccard	
	M	SD_V	M_P	SD_P
ResNet-50-LSTM ^b , $L = 8$ (similar to SV-RCNet [22])	0.881	0.063	0.739	0.090
TeCNO [16], <i>results of</i> [27]	0.886	0.078	0.751	0.069
TMRNet w/ ResNeST [40]	0.901	0.076	0.791	0.057
Trans-SVNet [27]	0.903	0.071	0.793	0.066
Not E2E [36]	0.920	0.053	0.771	0.115
SAHC [29]	0.918	0.081	0.812	0.055
ConvNeXt-LSTM ^b , $L = 256$ [23]	0.935	0.065	0.829	0.101
TUNeS, $L = 64$	0.938	0.052	0.838	0.085

Like prior art, we report the mean M and the standard deviation over videos SD_V for R-Accuracy. For R-Jaccard, we report the mean over phase-wise means M_P and the standard deviation over phases SD_P .

Model	Accuracy ^a	Macro Jaccard ^a	$F1$ score ^a
ResNet-50-LSTM ^b , $L = 8$	0.872 ± 0.004	0.707 ± 0.007	0.832 ± 0.003
TeCNO [16]			
<i>results of</i> [10]	0.874 ± 0.014	–	0.825 ± 0.018
<i>results of</i> [46]	0.900	0.723	0.839
Trans-SVNet [27]			
<i>results of</i> [46]	0.896	0.731	0.845
GRU w/ VideoSwin [11]	0.909	–	0.853
PATG w/ SE-ResNet-50 [37]	<u>0.914</u>	–	0.854
Dual Pyramid ASFormer w/ PCPVT [46]	<u>0.914</u>	<u>0.754</u>	<u>0.858</u>
TUNeS, $L = 64$	0.927 ± 0.004	0.796 ± 0.005	0.888 ± 0.003

^aThe reported sample standard deviation refers to the variation over repeated experimental runs.

^bTrained end-to-end on short video sequences of L frames.

- Train without token masking
- Train without feature sequence augmentation
- Omit self-attention and feedforward network in the Transformer blocks, thus keeping only the convolutional blocks
- For the offline model: Do not apply any attention masks in the Transformer blocks, thus do not constrain the Transformer to process past and future information separately
- Use different numbers n of Transformer blocks, where $n \in \{2, 4, 6, 8, 10\}$

In these experiments, we also used the learning rate scheduler with cosine decay and selected the model after the last epoch. This way, TUNeS's results on the 32:8:40 split improved slightly: Accuracy increased from 0.919 to 0.922 in online mode and from 0.941 to 0.945 in offline mode ($L = 64$).

V. DISCUSSION

As hypothesized, training the feature extractor in context proved beneficial: **All temporal models performed better on top of feature extractors that were trained with longer temporal context** (Fig. 1). Apparently, training in context helps the CNN to learn meaningful features that hold crucial information for subsequent analysis using a temporal model.

Training in context is simple to implement and does not require additional manual annotations such as tool labels. Also, it does not take more time than the standard frame-wise

TABLE II

OFFLINE RECOGNITION ON CHOLEC80. COMPARISON TO RESULTS FROM THE LITERATURE.

Model	R-Accuracy		R-Precision		R-Recall		split
	M	SD_V	M_P	SD_P	M_P	SD_P	
ASTCFormer [45]	0.957	0.033	0.923	0.062	0.912	0.095	40:20:20
TUNeS, $L = 64$	0.963	0.023	0.936	0.069	0.940	0.048	40:20:20

Like prior art, we report the mean M and the standard deviation over videos SD_V for R-Accuracy. For R-Precision and R-Recall, we report the mean over phase-wise means M_P and the standard deviation over phases SD_P .

Model	Accuracy ^a	Macro Jaccard ^a	$F1$ score ^a	split
GRU w/ VideoSwin [11]	0.939	–	0.898	40:40
TUNeS, $L = 64$	0.945 ± 0.005	0.829 ± 0.009	0.909 ± 0.005	40:40
Transition Retrieval Network [39]	0.901	–	0.848	40:20:20
TUNeS, $L = 64$	0.951 ± 0.004	0.835 ± 0.009	0.912 ± 0.005	40:20:20

^aThe reported sample standard deviation refers to the variation over repeated experimental runs.

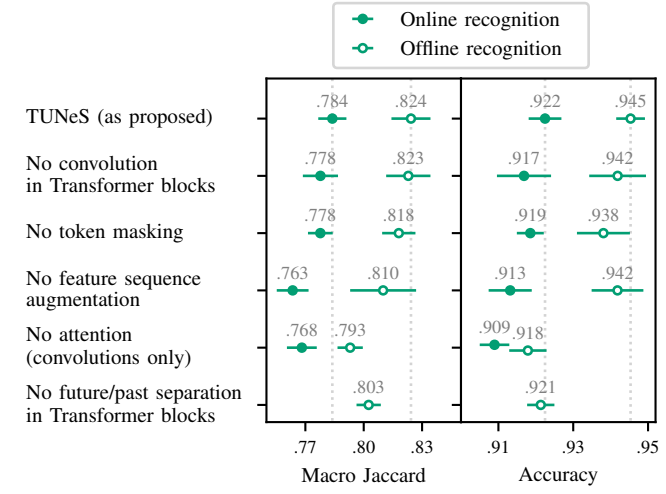


Fig. 10. Results on the Cholec80 data set (32:8:40 split) achieved when ablating different TUNeS components. All models are trained on features with $L = 64$. Error bars indicate the standard deviation over repeated experimental runs.

training. The only requirement is the availability of sufficient GPU memory (32 GB in our experiments).

When evaluating the baselines (Fig. 1), we found that the 2-layer GRU and OperA achieved subpar results. For the GRU, a reason could be that regularization with the smoothing loss and the proposed feature sequence augmentation was not as effective for this type of recurrent, sequential model. At least, the 2-layer GRU performed similarly to the TeCNO model that was trained without this regularization. Adding more layers to the GRU also did not improve results.

For OperA, we presume that the model is suffering from a lack of local inductive bias and struggles to filter information from noisy features. We observe that OperA improved considerably on contextualized features ($L = 64$), which might be more meaningful and thus easier to analyze with attention. We

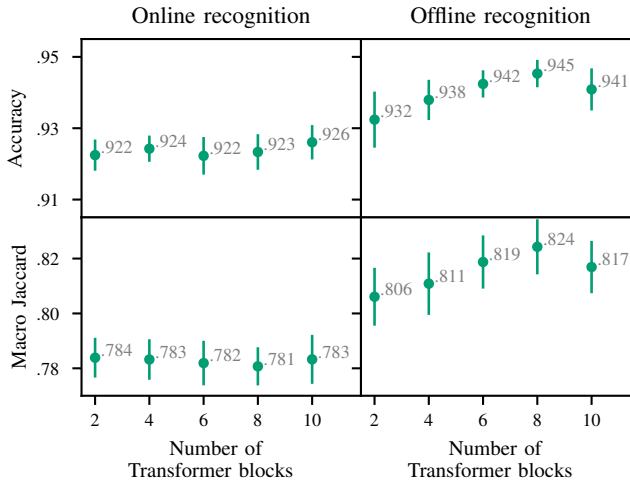


Fig. 11. Results on the Cholec80 data set (32:8:40 split) achieved by TUNeS models with varying numbers of Transformer blocks, trained on features with $L = 64$. Error bars indicate the standard deviation over repeated experimental runs.

want to note that we used a custom implementation of OperA here because the official code has not been released yet.

Further, in our experiments, training the Trans-SVNet blocks on top of TeCNO improved the results only marginally. Yet, compared to the original Trans-SVNet implementation, we used different hyperparameters for TeCNO (9 instead of 8 layers per stage, $\text{dim} = 64$ instead of $\text{dim} = 32$) and trained TeCNO for up to 75 epochs instead of only 8. We assume that Trans-SVNet mostly learns to locally smooth the TeCNO outputs, which may not be necessary when TeCNO has been tuned and trained properly.

The best performing baselines were TeCNO, SAHC, and ASFormer. **TUNeS outperformed the baselines in terms of accuracy and scored better or similarly on Macro Jaccard.** The results achieved by TUNeS, trained on top of the feature extractor with $L = 64$, also compare favorably to previous results from the literature (Tables I and II). In particular, on the 40:40 split, TUNeS achieved a mean video-wise accuracy of 0.927 and a mean video-wise Macro Jaccard of 0.796 for online recognition. For offline recognition, TUNeS achieved a mean video-wise accuracy of 0.945 and a mean video-wise Macro Jaccard of 0.829.

Moreover, **TUNeS is computationally efficient and scales well on long sequences** of up to two hours, regarding both latency and memory consumption (Fig. 9). In particular, TUNeS is faster than SAHC and than TeCNO. OperA has even lower latency, but struggles with increased memory usage on long sequences due to the quadratic memory complexity of attention. In contrast, ASFormer uses a custom implementation of local attention to restrict the memory consumption, which comes at the cost of increased computation times, especially on long sequences. Due to the sequential computation, GRU is also relatively slow on long sequences.

Regarding the number of model parameters, TUNeS belongs to the larger models with 1.13 M parameters. However, the feature extractor (ResNet-50) alone has 28.8 M parameters, making the size of the temporal model negligible. Further,

in online mode, where fewer Transformer blocks are used, TUNeS has only 580 K parameters.

When scaling the number of Transformer blocks (Fig. 11), we found that using more Transformer blocks was helpful for offline recognition but not for online recognition. Generally, it might be difficult to further improve on the online task due to the inherent uncertainty and ambiguity caused by the fact that the video stream is only partially available for analysis.

In the ablation experiments on TUNeS (Fig. 10), we checked the importance of both measures for regularization: token masking and feature sequence augmentation. Skipping token masking deteriorated the results only slightly. In contrast, skipping feature sequence augmentation had more of a negative effect, especially for online recognition. Here, Macro Jaccard dropped by 2.7 %. For offline recognition, however, feature sequence augmentation did not seem similarly important. Here, Macro Jaccard dropped only by 1.7 %.

In addition, we investigated the effect of both submodules in the TUNeS Transformer block: the convolutional block and the attention. Skipping the convolutional block did not lead to considerably worse results. Probably, the convolutional blocks in the encoder are sufficient to encode local inductive bias. However, **skipping the attention mechanism, together with the feedforward network, deteriorated the results noticeably**. Here, Macro Jaccard dropped by 2.0 % for online recognition and by 3.8 % for offline recognition. These results (without attention) are actually very close to the results achieved by TeCNO, indicating that multi-scale modeling alone cannot explain the success of TUNeS. Rather, including attention mechanisms to model global temporal relationships is decisive for the performance of TUNeS.

Furthermore, **masking attention so that past and future are processed separately in offline mode is important**. Without this kind of future/past separation, the model performed only slightly better than the model that used no attention at all. We want to note that we also used future/past separation for OperA in offline mode because the model failed to learn otherwise. Similarly, He *et al.* [11] had reported difficulties to train a 1-layer Transformer encoder for offline recognition.

VI. CONCLUSION

In this paper, we presented TUNeS, an effective and computationally efficient temporal model for phase recognition, which is applicable for both online and offline recognition.

In addition, we proposed a simple method for training a standard CNN with long temporal context to extract more meaningful visual features for surgical phase recognition at no additional computational cost.

Although TUNeS uses Transformer blocks to model long-range temporal relationships, it does not require hand-crafted local attention patterns or custom attention regularization losses. Instead, it uses specific strategies to incorporate attention mechanisms in a beneficial way. In particular, TUNeS (1) uses convolutions for pre-processing the input feature sequence to encode a local inductive bias, and thus (2) applies attention only to pre-filtered, downsampled, contextualized feature sequences. Further, (3) the Transformer blocks process

past and future information alternately to maintain a notion of temporal order in offline mode.

APPENDIX

A. Model and training details

1) Feature extractor: We used the *AdamW* optimizer [62] and a *one-cycle learning rate schedule* [63] with a maximum learning rate of $3 \cdot 10^{-4}$ and a constant weight decay of 0.01. The model after the last training epoch was used for feature extraction. To save on GPU memory, we finetuned only the upper two blocks (`conv4_x` and `conv5_x`) of the ResNet-50. Video frames were obtained at a resolution of 400×225 pixels and then cropped to 384×224 pixels. For data augmentation, we used the *Albumentations* library [64] to apply stochastic transformations to the video frames, including color and contrast modifications, blurring, geometric transformations, and horizontal flipping.

2) TUNeS: We trained with learning rate $\eta = 5 \cdot 10^{-4}$. For the baseline comparisons on the 32:8:40 split, we selected the model that achieved the best Macro Jaccard on the validation set. Otherwise, we applied cosine decay to the learning rate and selected the model after the final training epoch for evaluation. For convenience, all feature sequences were padded to a length that is divisible by 18.

3) GRU [7]: We used a GRU network with two layers and trained with learning rate $\eta = 1 \cdot 10^{-3}$. For offline recognition, we used a bidirectional 2-layer GRU.

4) TeCNO [16]:¹ We used two stages with 9 layers each in online mode and, to increase the size of the receptive field, 11 layers in offline mode.

5) ASFormer [28] (offline only):² For comparability with TeCNO, we used one decoder to obtain two stages in total. Per stage, we used 11 layers. To conform with the original codebase, we trained with a weight decay of $1 \cdot 10^{-5}$ and applied channel dropout ($p = 0.3$) [65] to the input features.

6) SAHC [29]:³ We used 11 layers in the initial stage and 10 layers in the following three refinement stages. To conform with the original code base, we trained SAHC for 100 epochs with a weight decay of $1 \cdot 10^{-5}$ and an initial learning rate of $5 \cdot 10^{-4}$, which was halved every 30 epochs. In addition, we used $\lambda_{\text{smooth}} = 1.0$, no class weights in the cross-entropy loss, no gradient clipping, and channel dropout ($p = 0.5$) on the input features. Note that we adjusted the model to use causal downsampling operations and causal attention in online mode and acausal convolutions in offline mode.

7) OperA [26]: We implemented OperA as a stack of 11 standard Transformer blocks (see Fig. 2a) with one attention head and 256 hidden units in the feedforward network. We trained with $\eta = 1 \cdot 10^{-4}$ and the additional attention regularization loss proposed in [26]. For offline recognition, we alternately masked future and past as proposed for TUNeS.

8) Trans-SVNet [27] (online only):⁴ We trained the Trans-SVNet modules on top of frozen TeCNO models with two

stages and 9 layers per stage. Following the original code base, we trained Trans-SVNet for 25 epochs with $\eta = 1 \cdot 10^{-3}$, using no class weights in the cross-entropy loss and no gradient clipping. In each experimental run, the TeCNO model and the Trans-SVNet with the best validation accuracy, respectively, were selected. Further, both the TeCNO model and the Trans-SVNet part were trained without feature sequence augmentation and without smoothing loss ($\lambda_{\text{smooth}} = 0.0$).

9) Loss functions:

$$\mathcal{L}_{\text{CE}}(\hat{y}, y) = -\frac{1}{T} \sum_{t=1}^T \gamma_{y_t} \cdot \log S(\hat{y}_t)_{y_t} \quad (4)$$

$$\mathcal{L}_{\text{smooth}}(\hat{y}) = \frac{1}{(T-1)C} \sum_{t=2}^T \sum_{p=1}^C \min(\Delta_{t,p}, \tau)^2, \text{ where} \quad (5)$$

$$\Delta_{t,p} = |\log S(\hat{y}_t)_p - \text{sg}(\log S(\hat{y}_{t-1})_p)|$$

$$\mathcal{L}_{\text{BCE}}(\hat{y}, y) = -\frac{1}{TC} \sum_{t=1}^T \sum_{p=1}^C (\gamma_p \cdot y_{t,p} \cdot \log(\sigma(\hat{y}_{t,p}))) + (1 - y_{t,p}) \cdot \log(1 - \sigma(\hat{y}_{t,p})) \quad (6)$$

Here, σ refers to the sigmoid function, S refers to the Softmax function, i.e., $S(\hat{y}_t)_p = \exp \hat{y}_{t,p} / \sum_{c=1}^C \exp \hat{y}_{t,c}$, sg refers to the stopgradient operator, which turns its operand into a constant with zero gradients, τ is a threshold that is set to 4, and γ_p , $1 \leq p \leq C$, refers to the class weight for phase p .

B. Additional results

TABLE III
COMPREHENSIVE RESULTS ON THE CHOLEC80 BENCHMARK,
ACHIEVED BY TUNeS WHEN TRAINED ON FEATURES WITH $L = 64$.

Metric	M	Online recognition		Offline recognition	
		32:8:40	40:40	32:8:40	40:40
Accuracy	M	0.922	0.927	0.945	0.945
	SD_V	0.057	0.051	0.036	0.035
	SD_R	0.004	0.004	0.004	0.005
Precision	M	0.877	0.886	0.906	0.911
	SD_V	0.057	0.052	0.049	0.045
	SD_P	0.084	0.082	0.073	0.068
	SD_R	0.004	0.003	0.005	0.005
Recall	M	0.884	0.890	0.902	0.908
	SD_V	0.062	0.053	0.054	0.043
	SD_P	0.075	0.062	0.079	0.064
	SD_R	0.006	0.004	0.009	0.008
Jaccard	M	0.783	0.795	0.823	0.828
	SD_V	0.084	0.074	0.075	0.067
	SD_P	0.115	0.110	0.110	0.101
	SD_R	0.007	0.005	0.010	0.009
Macro F1	M	0.860	0.870	0.887	0.892
	SD_V	0.065	0.055	0.058	0.049
	SD_R	0.005	0.004	0.008	0.007
Macro F1	M	0.880	0.887	0.904	0.909
	SD_V	0.053	0.045	0.047	0.039
	SD_R	0.004	0.003	0.006	0.005

For each metric, we report the mean M , standard deviation over videos SD_V , standard deviation over phases SD_P (if applicable), and standard deviation over runs SD_R . The video-wise Macro F1 is the average of the phase-wise F1 scores computed on one video. In contrast, the video-wise Macro F1 is the harmonic mean of Macro Precision and Macro Recall computed for one video.

¹Code based on <https://github.com/yabufarha/ms-tcn>

²Code based on <https://github.com/ChinaYi/ASFormer>

³Code based on <https://github.com/xmed-lab/SAHC>

⁴Code based on <https://github.com/xjgaocs/Trans-SVNet>

TABLE IV

ONLINE RECOGNITION ON CHOLEC80 (32:8:40 SPLIT) USING FEATURE EXTRACTORS WITH DIFFERENT TEMPORAL CONTEXT L .

Model	Accuracy ^a	Macro Jaccard ^a
$L = 1$		
ResNet-50	0.816 ± 0.003	0.591 ± 0.005
TeCNO*	0.877 ± 0.006	0.705 ± 0.016
Trans-SVNet*	0.879 ± 0.007	0.705 ± 0.018
GRU	0.875 ± 0.005	0.701 ± 0.011
OperA	0.863 ± 0.009	0.659 ± 0.013
SAHC	0.882 ± 0.006	0.718 ± 0.017
TeCNO	0.891 ± 0.004	0.730 ± 0.009
TUNeS	0.896 ± 0.006	0.739 ± 0.008
TUNeS ^b	0.894 ± 0.007	0.738 ± 0.010
$L = 8$		
ResNet-50-LSTM	0.865 ± 0.003	0.693 ± 0.007
ResNet-50-LSTM (<i>CHE</i>)	0.878 ± 0.007	0.713 ± 0.012
TeCNO*	0.883 ± 0.005	0.721 ± 0.011
Trans-SVNet*	0.889 ± 0.008	0.723 ± 0.027
GRU	0.879 ± 0.005	0.704 ± 0.011
OperA	0.880 ± 0.008	0.680 ± 0.013
SAHC	0.892 ± 0.012	0.736 ± 0.017
TeCNO	0.900 ± 0.004	0.750 ± 0.008
TUNeS	0.910 ± 0.007	0.759 ± 0.014
TUNeS ^b	0.912 ± 0.004	0.761 ± 0.010
$L = 64$		
ResNet-50-LSTM	0.901 ± 0.007	0.758 ± 0.012
ResNet-50-LSTM (<i>CHE</i>)	0.893 ± 0.021	0.723 ± 0.026
TeCNO*	0.898 ± 0.005	0.750 ± 0.010
Trans-SVNet*	0.898 ± 0.008	0.749 ± 0.014
GRU	0.901 ± 0.007	0.759 ± 0.012
OperA	0.898 ± 0.015	0.745 ± 0.015
SAHC	0.913 ± 0.010	0.779 ± 0.016
TeCNO	0.906 ± 0.008	0.768 ± 0.013
TUNeS	0.919 ± 0.007	0.782 ± 0.009
TUNeS ^b	0.922 ± 0.004	0.784 ± 0.007

^aThe reported sample standard deviation refers to the variation over repeated experimental runs.

^bWith *cosine annealing* learning rate scheduler, testing the model after the final training epoch.

*No feature sequence augmentation, no smoothing loss.

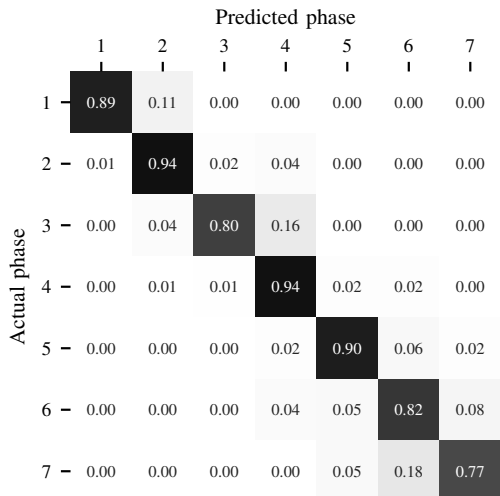


Fig. 12. Confusion matrix of the predictions of TUNeS ($L = 64$) on Cholec80 (32:8:40 split) in online mode. The confusion matrix is computed over all frames in the test set and all 25 experimental runs and then normalized by row. The entries on the diagonal present the frame-wise Recall for each phase, averaged over runs.

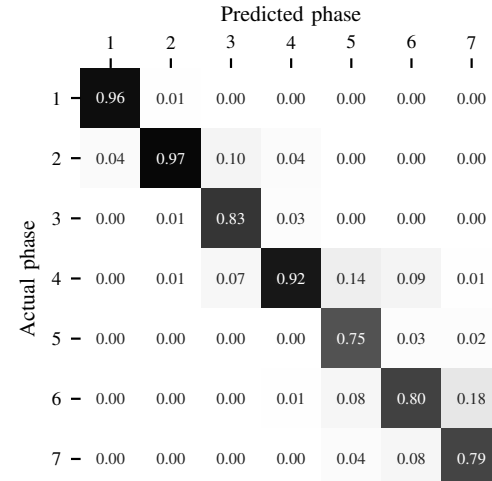


Fig. 13. Confusion matrix of the predictions of TUNeS ($L = 64$) on Cholec80 (32:8:40 split) in online mode. The confusion matrix is computed over all frames in the test set and all 25 experimental runs and then normalized by column. The entries on the diagonal present the frame-wise Precision for each phase, averaged over runs.

TABLE V
OFFLINE RECOGNITION ON CHOLEC80 (32:8:40 SPLIT) USING FEATURE EXTRACTORS WITH DIFFERENT TEMPORAL CONTEXT L .

Model	Accuracy ^a	Macro Jaccard ^a
$L = 1$		
GRU	0.881 ± 0.007	0.708 ± 0.011
OperA	0.873 ± 0.009	0.677 ± 0.014
SAHC	0.898 ± 0.004	0.750 ± 0.011
TeCNO	0.909 ± 0.005	0.779 ± 0.012
ASFormer	0.918 ± 0.004	0.797 ± 0.011
TUNeS	0.923 ± 0.008	0.790 ± 0.016
TUNeS ^b	0.922 ± 0.011	0.783 ± 0.016
$L = 8$		
GRU	0.902 ± 0.005	0.749 ± 0.011
OperA	0.890 ± 0.007	0.703 ± 0.010
SAHC	0.909 ± 0.004	0.775 ± 0.008
TeCNO	0.917 ± 0.003	0.798 ± 0.007
ASFormer	0.922 ± 0.004	0.805 ± 0.008
TUNeS	0.933 ± 0.008	0.804 ± 0.020
TUNeS ^b	0.934 ± 0.007	0.804 ± 0.016
$L = 64$		
GRU	0.917 ± 0.007	0.788 ± 0.012
OperA	0.924 ± 0.008	0.784 ± 0.016
SAHC	0.920 ± 0.006	0.804 ± 0.011
TeCNO	0.920 ± 0.008	0.807 ± 0.011
ASFormer	0.928 ± 0.005	0.824 ± 0.008
TUNeS	0.941 ± 0.006	0.824 ± 0.014
TUNeS ^b	0.945 ± 0.004	0.824 ± 0.010

^aThe reported sample standard deviation refers to the variation over repeated experimental runs.

^bWith *cosine annealing* learning rate scheduler, testing the model after the final training epoch.

REFERENCES

[1] N. Padov, T. Blum, S.-A. Ahmadi, H. Feussner, M.-O. Berger, and N. Navab, “Statistical modeling and recognition of surgical workflow,” *Med Image Anal*, vol. 16, no. 3, pp. 632–641, 2012.

[2] L. Maier-Hein *et al.*, “Surgical data science – from concepts toward clinical translation,” *Med Image Anal*, vol. 76, p. 102306, 2022.

[3] A. Dosovitskiy *et al.*, “An image is worth 16x16 words: Transformers for image recognition at scale,” in *ICLR*, 2021.

[4] C. Lea, M. D. Flynn, R. Vidal, A. Reiter, and G. D. Hager, “Temporal convolutional networks for action segmentation and detection,” in *CVPR*. IEEE, 2017, pp. 1003–1012.

[5] Y. A. Farha and J. Gall, “MS-TCN: Multi-stage temporal convolutional network for action segmentation,” in *CVPR*. IEEE/CVF, 2019, pp. 3575–3584.

[6] S. Hochreiter and J. Schmidhuber, “Long short-term memory,” *Neural Comput.*, vol. 9, no. 8, pp. 1735–1780, 1997.

[7] K. Cho *et al.*, “Learning phrase representations using RNN encoder–decoder for statistical machine translation,” in *EMNLP*. ACL, 2014, pp. 1724–1734.

[8] K. He, X. Zhang, S. Ren, and J. Sun, “Deep residual learning for image recognition,” in *CVPR*. IEEE, 2016, pp. 770–778.

[9] J. Deng, W. Dong, R. Socher, L.-J. Li, K. Li, and L. Fei-Fei, “ImageNet: A large-scale hierarchical image database,” in *CVPR*. IEEE, 2009, pp. 248–255.

[10] T. Czempiel, A. Sharghi, M. Paschali, N. Navab, and O. Moharer, “Surgical workflow recognition: From analysis of challenges to architectural study,” in *ECCV Workshops*. Springer, 2022, pp. 556–568.

[11] Z. He, A. Mottaghi, A. Sharghi, M. A. Jamal, and O. Moharer, “An empirical study on activity recognition in long surgical videos,” in *ML4H*, vol. 193. PMLR, 2022, pp. 356–372.

[12] Z. Liu *et al.*, “Swin transformer: Hierarchical vision transformer using shifted windows,” in *ICCV*. IEEE/CVF, 2021, pp. 9992–10002.

[13] C. Feichtenhofer, “X3D: Expanding architectures for efficient video recognition,” in *CVPR*. IEEE/CVF, 2020, pp. 200–210.

[14] Z. Liu *et al.*, “Video swin transformer,” in *CVPR*. IEEE/CVF, 2022, pp. 3192–3201.

[15] A. P. Twinanda, S. Shehata, D. Mutter, J. Marescaux, M. de Mathelin, and N. Padov, “EndoNet: A deep architecture for recognition tasks on laparoscopic videos,” *IEEE Trans Med Imag*, vol. 36, no. 1, pp. 86–97, 2017.

[16] T. Czempiel *et al.*, “TeCNO: Surgical phase recognition with multi-stage temporal convolutional networks,” in *MICCAI*. Springer, 2020, pp. 343–352.

[17] S. Ramesh *et al.*, “Multi-task temporal convolutional networks for joint recognition of surgical phases and steps in gastric bypass procedures,” *Int J Comput Assist Radiol Surg*, vol. 16, pp. 1111–1119, 2021.

[18] R. Sanchez-Matilla, M. Robu, M. Grammatikopoulou, I. Luengo, and D. Stoyanov, “Data-centric multi-task surgical phase estimation with sparse scene segmentation,” *Int J Comput Assist Radiol Surg*, vol. 17, no. 5, pp. 953–960, 2022.

[19] S. Bodenstedt *et al.*, “Unsupervised temporal context learning using convolutional neural networks for laparoscopic workflow analysis,” *arXiv:1702.03684*, 2017.

[20] I. Funke, A. Jenke, S. T. Mees, J. Weitz, S. Speidel, and S. Bodenstedt, “Temporal coherence-based self-supervised learning for laparoscopic workflow analysis,” in *CARE CLIP OR 2.0 ISIC*. Springer, 2018, pp. 85–93.

[21] S. Ramesh *et al.*, “Dissecting self-supervised learning methods for surgical computer vision,” *Med Image Anal*, vol. 88, p. 102844, 2023.

[22] Y. Jin *et al.*, “SV-RCNet: Workflow recognition from surgical videos using recurrent convolutional network,” *IEEE Trans Med Imag*, vol. 37, no. 5, pp. 1114–1126, 2018.

[23] D. Rivoir, I. Funke, and S. Speidel, “On the pitfalls of batch normalization for end-to-end video learning: A study on surgical workflow analysis,” *arXiv:2203.07976*, 2022.

[24] D. Bahdanau, K. Cho, and Y. Bengio, “Neural machine translation by jointly learning to align and translate,” in *ICLR*, 2015.

[25] A. Vaswani *et al.*, “Attention is all you need,” in *NeurIPS*, vol. 30, 2017.

[26] T. Czempiel, M. Paschali, D. Ostler, S. T. Kim, B. Busam, and N. Navab, “OperA: Attention-regularized transformers for surgical phase recognition,” in *MICCAI*. Springer, 2021, pp. 604–614.

[27] X. Gao, Y. Jin, Y. Long, Q. Dou, and P.-A. Heng, “Trans-SVNet: Accurate phase recognition from surgical videos via hybrid embedding aggregation transformer,” in *MICCAI*. Springer, 2021, pp. 593–603.

[28] F. Yi, H. Wen, and T. Jiang, “ASFormer: Transformer for action segmentation,” in *BMVC*, 2022.

[29] X. Ding and X. Li, “Exploring segment-level semantics for online phase recognition from surgical videos,” *IEEE Trans Med Imag*, vol. 41, no. 11, pp. 3309–3319, 2022.

[30] O. Ronneberger, P. Fischer, and T. Brox, “U-Net: Convolutional networks for biomedical image segmentation,” in *MICCAI*. Springer, 2015, pp. 234–241.

[31] H. Kwon, W. Shim, and M. Cho, “Temporal U-Nets for video summarization with scene and action recognition,” in *ICCV Workshops*. IEEE/CVF, 2019, pp. 1541–1544.

[32] D. Hendrycks and K. Gimpel, “Gaussian error linear units (GELUs),” *arXiv:1606.08415*, 2016.

[33] A. P. Twinanda, “Vision-based approaches for surgical activity recognition using laparoscopic and RGBD videos,” Ph.D. dissertation, Université de Strasbourg, 2017.

[34] F. Yu and V. Koltun, “Multi-scale context aggregation by dilated convolutions,” in *ICLR*, 2016.

[35] A. v. d. Oord *et al.*, “WaveNet: A generative model for raw audio,” *arXiv:1609.03499*, 2016.

[36] F. Yi, Y. Yang, and T. Jiang, “Not end-to-end: Explore multi-stage architecture for online surgical phase recognition,” in *ACCV*. Springer, 2022, pp. 2613–2628.

[37] A. Kadkhodamohammadi, I. Luengo, and D. Stoyanov, “PATG: Position-aware temporal graph networks for surgical phase recognition on laparoscopic videos,” *Int J Comput Assist Radiol Surg*, vol. 17, no. 5, pp. 849–856, 2022.

[38] J. Hu, L. Shen, and G. Sun, “Squeeze-and-excitation networks,” in *CVPR*. IEEE/CVF, 2018, pp. 7132–7141.

[39] Y. Zhang, S. Bano, A.-S. Page, J. Deprest, D. Stoyanov, and F. Vasconcelos, “Retrieval of surgical phase transitions using reinforcement learning,” in *MICCAI*. Springer, 2022, pp. 497–506.

[40] Y. Jin, Y. Long, C. Chen, Z. Zhao, Q. Dou, and P.-A. Heng, “Temporal memory relation network for workflow recognition from surgical video,” *IEEE Trans Med Imag*, vol. 40, no. 7, pp. 1911–1923, 2021.

[41] H. Zhang *et al.*, “ResNeSt: Split-attention networks,” in *CVPR Workshops*. IEEE/CVF, 2022, pp. 2736–2746.

[42] C.-Y. Wu, C. Feichtenhofer, H. Fan, K. He, P. Krahenbuhl, and R. Girshick, “Long-term feature banks for detailed video understanding,” in *CVPR*. IEEE/CVF, 2019, pp. 284–293.

[43] S. Ioffe and C. Szegedy, “Batch normalization: Accelerating deep network training by reducing internal covariate shift,” in *ICML*, vol. 37. PMLR, 2015, pp. 448–456.

[44] Z. Liu, H. Mao, C.-Y. Wu, C. Feichtenhofer, T. Darrell, and S. Xie, “A ConvNet for the 2020s,” in *CVPR*. IEEE/CVF, 2022, pp. 11966–11976.

[45] B. Zhang *et al.*, “Surgical workflow recognition with temporal convolution and transformer for action segmentation,” *Int J Comput Assist Radiol Surg*, 2022.

[46] H.-B. Chen, Z. Li, P. Fu, Z.-L. Ni, and G.-B. Bian, “Spatio-temporal causal transformer for multi-grained surgical phase recognition,” in *EMBC*. IEEE, 2022, pp. 1663–1666.

[47] X. Chu *et al.*, “Twins: Revisiting the design of spatial attention in vision transformers,” in *NeurIPS*, vol. 34, 2021, pp. 9355–9366.

[48] T.-Y. Lin, P. Dollár, R. Girshick, K. He, B. Hariharan, and S. Belongie, “Feature pyramid networks for object detection,” in *CVPR*. IEEE, 2017, pp. 936–944.

[49] X. Chen, N. Mishra, M. Rohaninejad, and P. Abbeel, “PixelSNAIL: An improved autoregressive generative model,” in *ICML*. PMLR, 2018, pp. 864–872.

[50] J. Ho, A. Jain, and P. Abbeel, “Denoising diffusion probabilistic models,” in *NeurIPS*, vol. 33, 2020, pp. 6840–6851.

[51] O. Petit, N. Thome, C. Rambour, L. Themyr, T. Collins, and L. Soler, “U-Net Transformer: Self and cross attention for medical image segmentation,” in *MLMI*. Springer, 2021, pp. 267–276.

[52] K. T. Rajamani, P. Rani, H. Siebert, R. ElagiriRamaLingam, and M. P. Heinrich, “Attention-augmented U-net (AA-U-Net) for semantic segmentation,” *SIViP*, vol. 17, no. 4, pp. 981–989, 2023.

[53] Z. Kong, W. Ping, A. Dantrey, and B. Catanzaro, “Speech denoising in the waveform domain with self-attention,” in *ICASSP*. IEEE, 2022, pp. 7867–7871.

[54] J. Long, E. Shelhamer, and T. Darrell, “Fully convolutional networks for semantic segmentation,” in *CVPR*. IEEE, 2015, pp. 3431–3440.

[55] X. Chu *et al.*, “Conditional positional encodings for vision transformers,” in *ICLR*, 2021.

[56] D. Eigen and R. Fergus, “Predicting depth, surface normals and semantic labels with a common multi-scale convolutional architecture,” in *ICCV*. IEEE, 2015, pp. 2650–2658.

[57] J. Devlin, M.-W. Chang, K. Lee, and K. Toutanova, “BERT: Pre-training of deep bidirectional transformers for language understanding,”

in *NAACL-HLT*. ACL, 2019, pp. 4171–4186.

[58] M. Joshi, D. Chen, Y. Liu, D. S. Weld, L. Zettlemoyer, and O. Levy, “SpanBERT: Improving pre-training by representing and predicting spans,” *TACL*, vol. 8, pp. 64–77, 2020.

[59] I. Funke, D. Rivoir, and S. Speidel, “Metrics matter in surgical phase recognition,” *arXiv:2305.13961*, 2023.

[60] D. P. Kingma and J. Ba, “Adam: A method for stochastic optimization,” in *ICLR*, 2015.

[61] I. Loshchilov and F. Hutter, “SGDR: Stochastic gradient descent with warm restarts,” in *ICLR*, 2017.

[62] ——, “Decoupled weight decay regularization,” in *ICLR*, 2019.

[63] L. N. Smith and N. Topin, “Super-convergence: Very fast training of neural networks using large learning rates,” in *Artificial Intelligence and Machine Learning for Multi-Domain Operations Applications*, vol. 11006. SPIE, 2019, p. 1100612.

[64] A. Buslaev, V. I. Iglovikov, E. Khvedchenya, A. Parinov, M. Druzhinin, and A. A. Kalinin, “Albumentations: Fast and flexible image augmentations,” *Information*, vol. 11, no. 2, p. 125, 2020.

[65] J. Tompson, R. Goroshin, A. Jain, Y. LeCun, and C. Bregler, “Efficient object localization using convolutional networks,” in *CVPR*. IEEE, 2015, pp. 648–656.